Eliminating Quantum Phase Slips in Superconducting Nanowires

Jan Nicolas Voss,* Yannick Schön, Micha Wildermuth, Dominik Dorer, Jared H. Cole, Hannes Rotzinger,* and Alexey V. Ustinov

ABSTRACT: **In systems with reduced dimensions, quantum fluctuations have a strong influence on the electronic conduction, even at very low temperatures. In superconductors, this is especially interesting, since the coherent state of the superconducting electrons strongly interacts with these fluctuations and therefore is a sensitive tool to study them. In this paper, we report on comprehensive measurements of superconducting nanowires in the quantum phase slip regime. Using an intrinsic electromigration process, we have developed a method to lower the nanowire's resistance *in situ* and therefore eliminate quantum phase slips in small consecutive steps. We observe critical (Coulomb) blockade voltages and superconducting critical currents, in good agreement with theoretical models. Between these two regimes, we find a continuous transition displaying a nonlinear metallic like behavior. The reported intrinsic electromigration technique is not limited to low temperatures, as we find a similar change in resistance that spans over 3 orders of magnitude also at room temperature. Aside from superconducting quantum circuits, such a technique to reduce the resistance may also have applications in modern electronic circuits.**

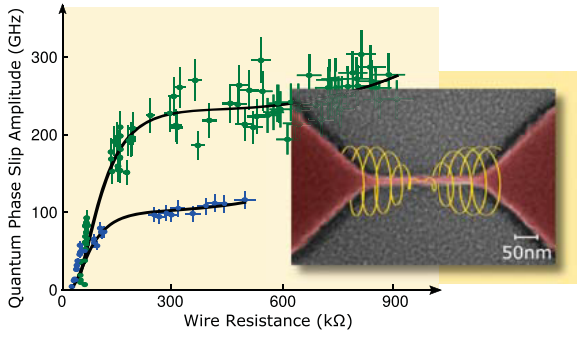

KEYWORDS: *nanowires, granular aluminum, quantum phase slips, Josephson weak links, resistance tuning*

When the dimensions of electronic circuits are reduced to nanometer scales, their transport characteristics can change fundamentally. A superconducting wire, which is approximately as narrow as the variation length scale of the superconducting order parameter, responds to an applied electrical field in dramatically different ways: The behavior of a short wire with a low normal state resistance resembles, at temperatures well below the critical temperature, the well known behavior of a bulk superconductor. The order parameter is well defined and the resistance vanishes. A long wire with a sufficiently high normal state resistance, instead, does not even reveal superconductivity at a first glance, since the wire does not conduct electrical current at low applied voltages.

This intriguing phenomenon has its origin in the strong confinement of the superconducting condensate which leads to a highly fluctuating order parameter, and therefore its phase 'slips'[1−5] (for an overview of the effect see, *e.g.*, ref 6). At temperatures close to the transition temperature, the electrical response is governed by thermally activated phase slips.[7,8] At very low temperatures, however, the origin of these phase slips has a quantum nature. Between the two extreme states, superconducting and insulating, the response shows a nonlinear metallic like behavior at small applied voltages (in the following for simplicity denoted as 'metallic').

To date, it was not possible to access these three different regimes at low magnetic fields with a single wire,[9−11] since the intrinsic properties, like coherence length or nanowire resistance, were fixed by the preparation of the wire.

In this paper, we present a technique which allows for the permanent reduction of the normal state resistance of single wires by 3 orders of magnitude compared to its initial resistance at low temperatures. We use current pulses of increasing amplitude to alter the internal structure of oxidized (granular) aluminum (AlO_x) nanowires by an intrinsic electromigration (IEM) process. By doing so, we observe a transition of the electrical response from the insulating through the metallic to the superconducting state.

The studied thin films consist of a network of small aluminum grains with a diameter of about 4 nm covered by a thin aluminum oxide insulator (see TEM picture in Supporting Information of ref 12). This intergrain matrix plays a dominant role in the transport properties of the material and, at very low temperatures where the aluminum is in the superconducting state, is usually described as a network of Josephson weak links. The charge transport between the grains and thus also the normal state resistance are therefore strongly dependent on the thickness of the insulating barriers. In the fabrication process of the films, the thickness of the insulating layer between the grains can be influenced by the amount of oxygen added to the deposited pure aluminum. These films can have a normal sheet resistance up to several kΩ and exhibit low intrinsic microwave losses in the superconducting state, making them a versatile material for high impedance superconducting quantum circuits (see, *e.g.*, refs 12−15). The kinetic inductance L_k of a wire made of such film may exceed the geometric inductance by orders of magnitude. It is convenient to describe it by $L_k = \hbar R_n/\pi\Delta = 0.18\hbar R_n/k_B T_c$, where R_n, Δ, T_c are the normal state resistance, the (BCS) superconducting energy gap, and the transition temperature (1.4−2 K for granular aluminum).[12]

Due to the Josephson coupling between the grains, the transport properties of AlO_x films are inherently nonlinear. However, if the number of parallel grains in a wire is large, the Josephson nonlinearity is washed out and becomes only visible at large electrical currents.

Theoretical Background. Neglecting the microscopic disorder, the transport dynamics of superconducting nanowires in the insulating regime has been proposed to be dual to the transport dynamics of a Josephson junction in the superconducting regime.[16] Following ref 17, a measure of the strength of the phase fluctuations in a wire is given by the phase slip energy:

$$E_s = \alpha\left(\frac{L_w}{\xi}\right)^2 k_B T_c \frac{R_q}{R_n}\exp\left(-\beta\frac{R_q L_w}{\xi R_n}\right) \quad (1)$$

where L_w, ξ, and $R_q = h/4e^2$ are the length of the wire, the effective superconducting coherence length, and the superconducting resistance quantum, respectively. The empirical constants α and β are of the order of 1.[17] The phase slip energy exponentially depends on the normal state resistance R_n. Thus, E_s can vary by orders of magnitude within the R_n range studied in this paper.

The inductive energy $E_L = \Phi_0^2/2L_k$ also plays an important role in the electrical response of a wire. If E_L is much larger than E_s, the superconducting phase difference along the wire is well defined, showing a superconducting behavior. Here, coherent transport of Cooper pairs leads to a vanishing voltage drop up to a critical current I_c; for a review see, *e.g.*, ref 18. In the insulating regime, where E_s is much larger than E_L, no conductance is observed up to an applied critical voltage of $V_c = 2\pi/2e\,E_s$. When altering R_n, both E_s and E_L are changed, E_L, however, only linearly:[17]

$$\frac{E_s}{E_L} = \alpha\left(\frac{L_w}{\xi}\right)^2 \frac{0.18}{\pi}\exp\left(-\beta\frac{R_q L_w}{\xi R_n}\right) \quad (2)$$

As a result, already small changes in R_n have a high impact on the ratio between E_s and E_L and thus on the transport properties of the wire. Following Mooij *et al.*,[17] the transition from an insulating to a superconducting behavior should happen at $E_s \approx 0.2\,E_L$.

RESULTS AND DISCUSSION

Reducing the Normal-State Resistance. Our experiments focus on a scheme of applying current pulses and measuring the changes in the normal state resistance R_n of a wire together with the current−voltage (I−V) characteristics in the superconducting state. Figure 1a shows a typical resistance

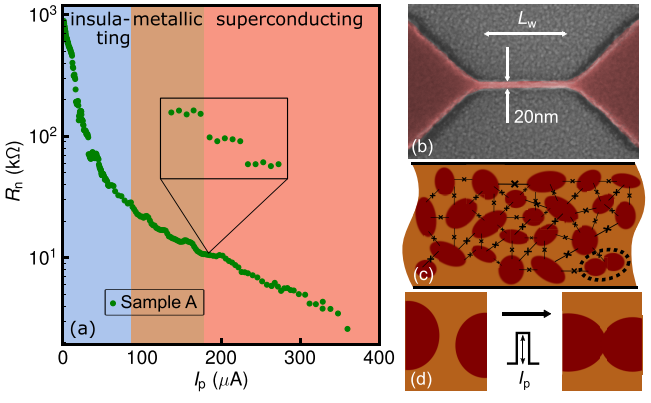

Figure 1. (a) Normal state resistance of an oxidized (granular) aluminum nanowire as a function of the applied pulse current I_p measured at 25 mK. The resistance of the 20 nm wide and 1000 nm long nanowire is stepwise (inset) lowered from 900 kΩ to 2.5 kΩ. At low bias values, an insulating, metallic, and superconducting behavior is observed. (b) Scanning electron micrograph of a lithographically fabricated nanowire (colored in red) on a sapphire substrate. (c) Illustration of the wire structure. Isolated aluminum grains (red, size ≃4 nm) are embedded in an aluminum oxide matrix (orange), forming a network of tunnel junctions (black crosses). (d) Proposed microscopic process: The current pulses lead to an IEM merging grains and/or clusters of grains.

R_n *vs* pulse amplitude I_p measurement at 25 mK here for sample A (length 1000 nm). We applied current pulses with increasing amplitudes ranging from $I_p \simeq 1$ μA to $I_p = 380$ μA in 240 steps. Once a reduction of R_n at a certain threshold current I_p is observed, applying pulses with an amplitude below the next threshold does not change R_n. This behavior is illustrated in the inset of Figure 1a. To study the impact of the pulse duration on the change in resistance, we applied pulses with varying lengths, ranging from milliseconds up to minutes. We observed no pulse duration effect at these time scales. After the resistance is changed to a certain R_n, it remains stable, also after thermal cycling of the cryostat to room temperature. In addition, to ensure that the altered resistance values as well as the transport characteristics are stable in time, test measurements were performed over days. Both the normal state resistance and the transport response did not change over time. We have applied the described measurement scheme at various temperatures to about 25 nanowire samples of different lengths and from different fabrication batches with similar results. Due to the character of the change in resistance, we name the method as IEM.

We suggest the following microscopical origin for the alteration of the resistances, illustrated in Figure 1d. With a current applied to the nanowire, a local voltage develops which mainly drops over the insulating grain to grain interlayers. At a threshold current I_p, the tunnel junction is pinched out, merging two or more grains with the weakest insulating

Table 1. Parameters of the Samples Measured at mK Temperatures[a]

no.	L_w (nm)	R_n^0 (kΩ)	R_n^E (kΩ)	R_n^m (kΩ)	R_n^s (kΩ)	R_n^0/R_n^E	E_s^0/h (GHz)	E_s^m/h (GHz)	E_s^s/h (MHz)	E_s^E/h (Hz)
A	1000	900	2.5	37	16	360	200	2.5	1	10×10^{-21}
B	750	500	3.7	28	17	135	164	3.0	34	10×10^{-7}
C	250	12.4	1.5	12.4	4.7	8.3	0.5	0.5	2.5×10^{-3}	10×10^{-16}

[a]All AlO_x nanowires have a width and a thickness of 20 nm. R_n^0 and R_n^E denote the initial and final normal state resistance (before and after altering the nanowire), and E_s^0 and E_s^E are the corresponding phase slip energies. R_n^m, E_s^m and R_n^s, E_s^s are the largest metallic and superconducting normal state resistances/phase slip energies.

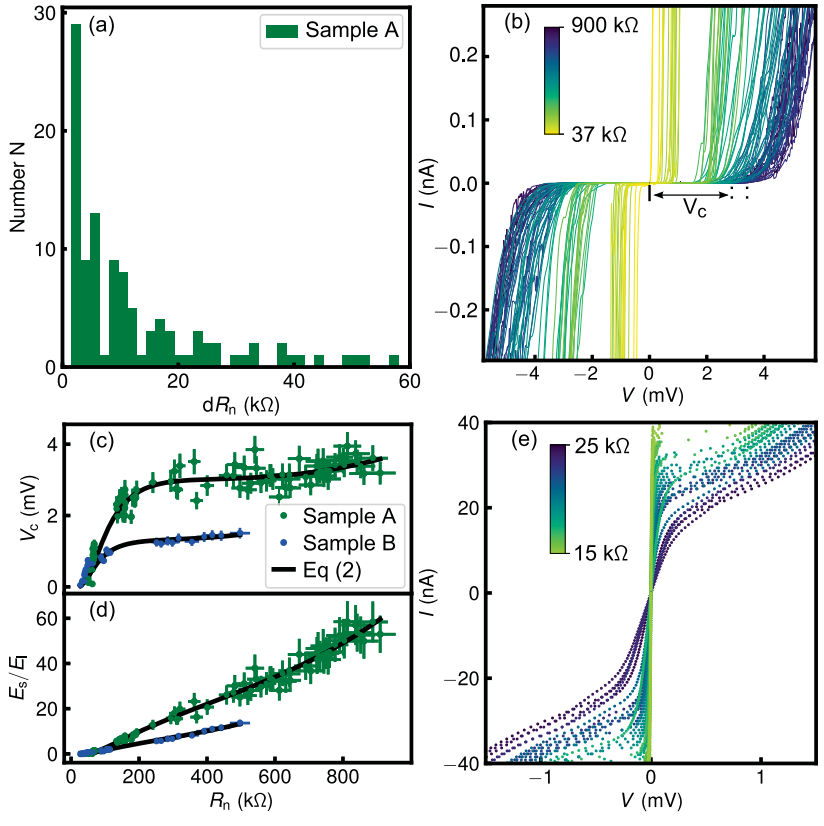

Figure 2. (a) Distribution of resistance steps dR_n for sample A. Steps of $dR_n > 20$ kΩ occur only at very small I_p. (b) $I-V$ characteristics for a 1000 nm long nanowire. Darker curves correspond to higher resistance values, brighter to lower. The Coulomb blockade range is from 3.6 mV for a normal state resistance of ≈800 kΩ down to about 0.1 mV for the lowest resistance value (≈40 kΩ). (c) Ratio between phase slip energy E_s and inductive energy E_L as a function of the normal state resistance of wires A and B. For both wires, the ratio converges for smaller resistances toward the same value. Here, the transition from insulating to metallic behavior occurs at $E_s/E_L \approx 0.02$. (d) Critical voltages V_c as a function of the normal state resistance R_n. The comparison of measured values and the predictions from eq 1 (b) and eq 2 (c) with the fitting parameters $\alpha = 0.07 \pm 0.01$ and $\beta = 0.49 \pm 0.03$ shows a good agreement for both wires (see black solid lines in (c) and (d)). (e) $I-V$ characteristics of sample A in the metallic regime (≈25 to 15 kΩ). In the vicinity of zero bias current, the slope increases when the wire resistance is reduced. The measurements were performed at 25 mK.

barrier.[19,20] We observe that the current pulses can be either applied at room temperature or at low temperatures with very similar results, leading to a permanent change in resistance. It is advantageous, especially at low temperatures to apply relatively short current or voltage pulses to avoid unnecessary heating. Our findings indicate that this procedure creates an altered network of more strongly connected grains, which effectively leads to an increase in the wire conductance, as seen in Figure 1a.

We note that both the magnitude of the R_n changes and the adjusting accuracy are dependent on the wire length (data not shown). The wire resistance tends to increase with length, but does not strictly scale with it. The reason for this lies in the disordered character of the internal structure of the wire. A qualitative explanation for this behavior may lie in the random distribution of barrier thicknesses. To first order, the number of junctions in the network scales linearly with the length of the nanowire. The probability of having a few very weak internal junctions dominating R_n therefore also increases quickly with the length (see Table 1). As a consequence, the first changes in resistance are very steep (Figure 1a). However, with a further reduction of resistance, we observe smaller steps. Figure 2a displays the distribution of resistance steps dR_n for sample A, hosting a few thousand separated aluminum grains.

Insulating Regime. By using the IEM method, the resistance values initially change rapidly (Figure 1a), and we observe larger gaps between the measured resistance values (order of 10 kΩ), visible as larger steps in the distribution tail in Figure 2a. Consequently, also the critical voltage values reflect these gaps in R_n.

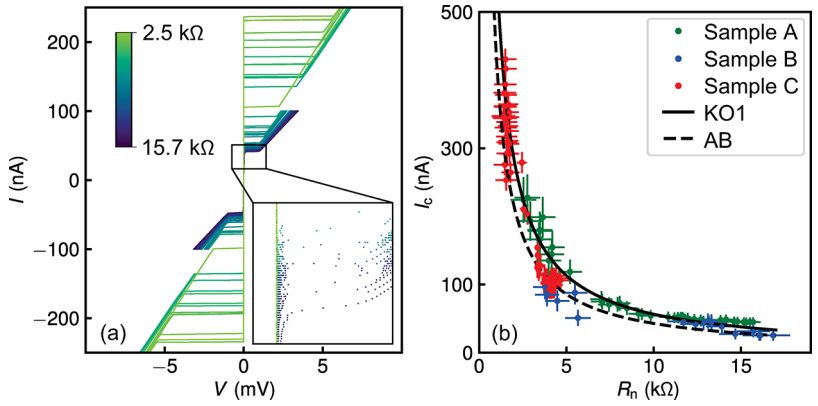

Figure 3. (a) $I-V$ characteristics of sample A as a function of normal state resistance. Here R_n is extracted from the resistive slope above I_c at finite voltages. (b) Critical currents, when the wires are in the superconducting regime, compared with the predicted values from the KO1 (black solid line) and AB (black dashed line) theory.

Prior to applying any current pulses to lower R_n, samples A and B, see Table 1, showed a strong Coulomb blockaded behavior with maximal critical voltage V_c = 3.6 mV (Figure 2d). For high blockade voltages, we observed a continuous rounding of the $I-V$ characteristics at V_c which lead to a significant error contribution in the determination of V_c values >2 mV ($E_s/h \approx 150$ GHz in the QPS model). We attribute this rounding to an effect of the relatively low impedance of the environment and therefore elevated temperature due to dissipation in the nanowire.[21] However, at lower V_c, the $I-V$ characteristics become very steep, but not hysteretic in the current values.

As an important consequence of the lowering of R_n, we expect the granular structure to be altered, forming a network of more and more galvanically connected grains (see Figure 1d). Due to reduced grain boundary scattering,[22] a longer mean free path l_0 also results in an increased coherence length $\xi_{eff} = \sqrt{l_0 \xi_0}$. Experimentally, this has also been observed in other granular and amorphous systems which have been grown under different conditions[23] or treated by electromigration.[24] The data presented in Figure 2c,d are best fitted assuming a linear ξ span from ξ = 8 nm (R_n = 900 kΩ) to ξ = 12 nm (R_n = 37 kΩ).

Figure 2d displays the extracted critical voltages as a function of the altered normal state resistances for both wires. The overlaid curve is a fit to the measured data using eq 1. The two extracted parameters $\alpha = 0.07 \pm 0.01$ and $\beta = 0.49 \pm 0.03$ are common to the data of samples A and B and in good agreement with the values given in ref 17. Figure 2c shows excellent agreement with the QPS theory, eq 2, for samples A and B. Here, we also took into account the change in the inductive energy. The ratio E_s/E_L drops almost linearly to values below unity where we find a transition to the metallic regime.

Metallic Regime. We observe a metallic regime for all samples with R_n values between 40 kΩ and 16 kΩ, characterized by a linear response for small bias values and a nonlinear response at larger bias values. For sample A, this is shown in Figure 2e, see also the Supporting Information. The exact nature of the metallic regime is currently not clear.

From the perspective of the QPS model, using the parameters evaluated above, in this regime the $I-V$ character istic is associated with E_s in the range between $E_s/h \approx 3$ GHz and $E_s/h \approx 30$ MHz, while E_L changes between $E_L/h \approx 150$ GHz and $E_L/h \approx 250$ GHz. In this intermediate regime, E_s reduces to values where on average neither the localization of charges in the wire nor the phase coherence across the wire is dominating.

The observed transitions from insulating to metallic and from metallic to superconducting behavior in our experiments are consistent with previous work on two dimensional (2D) granular films,[25] metal hybrids,[26] and one dimensional (1D) arrays of Josephson junctions. For a detailed discussion on the I−M−S transition in 2D granular superconductors, see refs 27−29. More recent studies of 1D chains and 2D arrays of Josephson junctions[30] have reported a similar behavior with transitions between insulating, metallic (quasiparticle domi nated), and Cooper pair dominated transport as a function of temperature and magnetic field.[31−34] The interplay between fundamental energy scales in these systems is similar to the granular aluminum films, and so one would expect similar transport properties.

If one considers the model of a network of Josephson junctions (illustrated in Figure 1c), there are two energy scales of interest. The finite charging energy of the grains sets the energy scale associated with localized charges in the system, whereas the Josephson energy sets the energy scale of the delocalization which underpins the superconducting state. One can argue that there should be a transition (even at zero temperature) associated with the crossover from Coulomb dominated to Josephson dominated dynamics, as is typically discussed in the context of Josephson junction arrays.[30] As more links are connected by the IEM, the charging energy per grain is reduced eventually allowing conduction pathways to form, resulting in a metallic state.

Superconducting Regime. For values of R_n/L_w (here L_w is the wire length) smaller than about 20 Ω/nm, the $I-V$ characteristics display a transition into a supercurrent state with no voltage drop up to a critical current I_c. In Figure 3a, this is shown for sample A. At the largest R_n and at current values close to I_c, the voltage drop across the wire develops rather smoothly (inset), very similar to the phase diffusion behavior of small capacitance Josephson junctions. Larger I_c values show a voltage discontinuity which develops in magnitude as R_n decreases, as it is common for super conducting wires.

Under the assumption that the QPS model is still valid and that the above determined empirical parameters α and β are unchanged, we can compute E_s to be of the order of 1 MHz,

while E_L can be a few hundred MHz. Due to the smallness of E_s, however, it is more useful to describe the wire as a narrow superconducting filament. Therefore, we compare the measured I_c to a model for short weak links in the dirty limit (mean free path $l_0 \ll L_{link}$) (Kulik and Omel'Yanchuk, KO1)[35] and to the expectation that the wire would behave like a Josephson tunnel junction (Ambegaokar and Baratoff, AB).[36] For details see the Supporting Information.

For both models, I_c as a function of the normal state resistance is given by $\langle I_c \rangle = g'(\pi\Delta_{BCS}/2e)\langle R_n \rangle^{-1}$ with $g' = 1.32$ (KO1) or $g' = 1$ (AB). Our measurements do not allow the determination of the current phase relation of the wire at a given resistance and thus cannot be compared with both models in this respect. Figure 3b shows the calculated values for both models, together with the I_cs from all three samples.

Connecting the picture with Josephson networks, we can interpret the M−S transition as the point at which the average Josephson energy is larger than the Coulomb energy, and the usual Bose gas/glass description would now apply. If the superconducting gap is suppressed in the smallest grains,[37] the fusing of grains will also have the effect of reducing the suppression, increasing the gap and further strengthening the superconducting phase.

Phase Diagram. We construct a tentative phase diagram by taking the smallest R_n values of sample A, which still show a zero current state, and the largest R_n value, which just shows a zero voltage state, and estimate the E_s/E_L ratio according to the QPS theory. By assuming that this ratio is the same for other samples, the thick black lines in Figure 4 indicate the phase transition for nanowires with differences in length and in R_ξ (normal state resistance per coherence length). The shortest wire, sample C, shows no insulating phase, which is consistent with the phase diagram. For comparison, we added the data from Bollinger *et al.*[38] together with the analysis from Mooij *et al.*[17] The measurement data of Bollinger *et al.* do not strictly distinguish between insulating and metallic, thus the data appear in Figure 4 in both the insulating and the metallic phase. For the studied wires, the transitions from superconducting (red dots) to metallic (gray dots) and further up to insulating state (blue dots) nicely coincide with the solid lines drawn for constant E_s/E_L ratios of 10^{-4} and 2×10^{-2}. Except for very short wires, we find a good agreement, especially if one takes the large parameter space, the very different material systems, and the employed techniques into account.

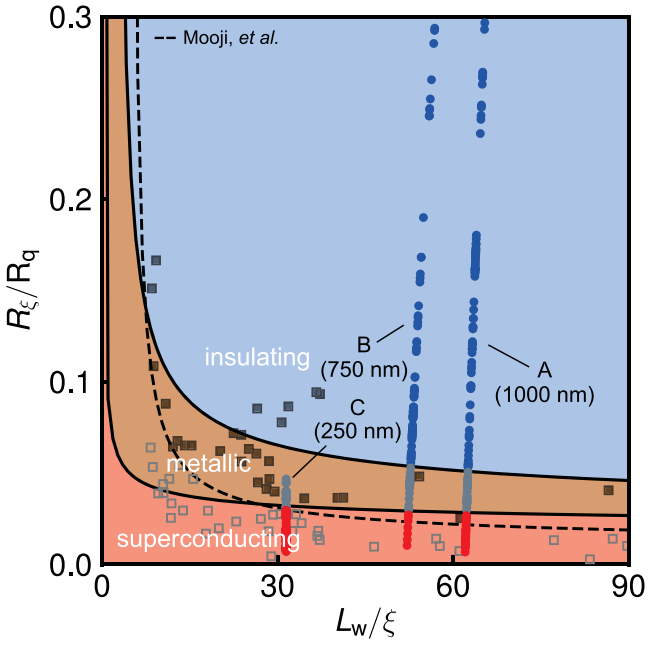

Figure 4. Tentative phase diagram for nanowires made from oxidized (granular) aluminum. For the black lines, the ratio between the phase slip energy and the inductive energy of the wires is constant for different geometries and specific resistances. The dots represent the altered normal state resistances and the color the low temperature state (blue = insulating, gray = metallic, red = superconducting). Assuming a constant wire geometry and only small changes in the coherence length, the ratio between E_s and E_L decreases together with R_ξ. From the smallest measurable critical voltages, we find a constant ratio of $E_s/E_L \approx 0.02$ (see Figure 2b) for the insulating to metallic transition (upper black line). The ratio at which the transition, metallic to superconducting, occurs ($E_s/E_L \approx 10^{-4}$, lower black line), is determined from the smallest R_n values in the superconducting regime. For both transition lines, the previously determined values of $\alpha = 0.07$ and $\beta = 0.49$ have been used. The black and gray squares represent the data from Bollinger *et al.*[38] and the model is taken from ref 17.

CONCLUSIONS

In this paper, we have demonstrated that the normal state resistance of narrow nanowires made from oxidized (granular) aluminum can be reduced *in situ* at low temperatures by using current pulses. This tuning allowed us to observe a transition from insulating to superconducting behavior in a very controlled way, showing good agreement with theoretical models. We also report on the observation of a pronounced metallic behavior characterized by strongly nonlinear conductance which is located between the insulating and the superconducting phases. The demonstrated intrinsic electromigration process of the granular aluminum also provides a powerful method of probing the superconductor to insulator transition. Using the QPS model, we proposed a tentative phase diagram, predicting the transition parameters.

Apart from basic questions addressing superconducting nanowires, the results of this work may have impacts on more applied topics. The demonstrated strong nonlinearity of the wires—in conjunction with their low loss and their large kinetic inductance—make them promising elements for superconducting quantum circuits,[3,15,21,39,40] qubits, and metamaterials. Furthermore, particle detectors such as microwave kinetic inductance detectors or superconducting nanowire single photon detectors may be optimized using the adjustability of the nanowire's resistance, as described in this work.

EXPERIMENTAL METHODS

The nanowires are fabricated from a 20 nm thick AlO_x film deposited on a sapphire substrate; see Figure 1b for a scanning electron microscope image. The film has a sheet resistance of 2.7 kΩ and T_c = 1.8 K. We use a single argon/chlorine based anisotropic etching step and a hydrogen silsesquioxane/poly(methyl methacrylate) bilayer etch mask to define the wire and the leads to the wire.[12,15] The wires have a nominal width of 20 nm.

The three measured nanowire samples are located on the same chip. Each wire has AlO_x leads with a width of 0.5 and 2.5 μm length that contribute to an inductance of 20 nH. With a stray capacitance of about 45 fF, we estimate an environmental impedance of about 0.6 kΩ, not considering the inductance of the nanowire itself.

The measurements were carried out in a dilution refrigerator at a temperature of 25 mK. The electric bias leads are filtered at several stages from room temperature to the base temperature with copper

powder, π, and RCR low pass filters leading to an effective measurement bandwidth of about 5 kHz. In the insulating regime, however, the $I-V$ characteristics are measured for a better signal to noise ratio with a minimal sampling time of about 0.02 s. For the superconducting (low impedance) and insulating (high impedance) regimes, we use different amplifier readout schemes (see Supporting Information for additional information).

A computer controlled measurement protocol was carried out for all samples in the following way: First, the $I-V$ characteristics were measured in either a voltage bias scheme (insulating regime) or a current biased scheme (metallic and superconducting regime). Then I_p was applied for about 20 ms followed by at least a few seconds waiting time to allow the samples to recover into thermal equilibrium. The nanowire resistance R_n was determined with an excitation current below I_p. This then was followed by the next $I-V$ measurement cycle, and so on.[41]

The wire resistance is given by $R_n = R_{tot} - R_L - R_{th}$, where R_{tot} is the total value of the resistance measured, $R_L = 26.5$ kΩ (samples A and C) and $R_L = 39$ kΩ (sample B) are the resistances of the on chip leads connecting the nanowires. R_L is in very good agreement with estimates using the AlO_x sheet resistance and the geometry of the leads.

We also recognized a 'thermal' resistance offset R_{th} at larger current bias values which is of the order of 15 kΩ and can be explained by considering Joule heating.[10]

In the insulating and metallic regime, the resistances were determined from I_p. In the superconducting regime, however, R_n was extracted from the resistive slopes of the $I-V$ characteristics above I_c which conveniently allows to determine R_L and R_{th}.

The effective coherence length ξ was extracted from temperature dependent measurements of the upper critical magnetic field H_{c2} for several μm wide AlO_x wires with a sheet resistance ranging from 2.0 kΩ to 5.1 kΩ. We found a constant $H_{c2}(T = 0) = 4.5 \pm 0.2$ T/μ_0, consistent with ref 42. From this result, we get $\xi_n^0 = 8 \pm 0.4$ nm, which is in good accordance with the 10 nm value quoted in refs 43 and 44. We take ξ_n^0 as a starting point for unaltered highly resistive nanowires. We assume furthermore that the wire cross section is sufficiently homogeneous and that the wire's E_s is not dominated by a narrow constriction in the nanowire. However, possible defects cannot be ruled out completely. In electron microscopy scans, the wires appear smooth and uniform with an edge roughness of the order of 1−2 nm.

AUTHOR INFORMATION

Corresponding Authors

Jan Nicolas Voss − *Physikalisches Institut, Karlsruher Institut für Technologie, 76131 Karlsruhe, Germany;* orcid.org/0000 0002 9929 0305; Email: voss@kit.edu

Hannes Rotzinger − *Physikalisches Institut and Institute for Quantum Materials and Technologies, Karlsruher Institut für Technologie, 76131 Karlsruhe, Germany*; Email: rotzinger@kit.edu

Authors

Yannick Schön − *Physikalisches Institut, Karlsruher Institut für Technologie, 76131 Karlsruhe, Germany;* orcid.org/0000 0002 2448 7664

Micha Wildermuth − *Physikalisches Institut, Karlsruher Institut für Technologie, 76131 Karlsruhe, Germany*

Dominik Dorer − *Physikalisches Institut, Karlsruher Institut für Technologie, 76131 Karlsruhe, Germany*

Jared H. Cole − *Chemical and Quantum Physics, School of Science, RMIT University, Melbourne, Victoria 3000, Australia*

Alexey V. Ustinov − *Physikalisches Institut and Institute for Quantum Materials and Technologies, Karlsruher Institut für Technologie, 76131 Karlsruhe, Germany; National University of Science and Technology MISIS, Moscow 119049, Russia; Russian Quantum Center, Moscow 143025, Russia*

Author Contributions

J.N.V. and H.R. conceived the idea and designed the experiments. J.N.V., M.W., and H.R. conducted the measurements. J.N.V., Y.S., and D.D. did the fabrication. The data analysis was done by J.N.V. and H.R., with support from J.H.C. All authors contributed to the discussions and interpretations of the results. The project was supervised by H.R. and A.V.U.

Notes

The authors declare no competing financial interest.

A preprint version of the manuscript was submitted to arXiv: Voss, J. N.; Schön, Y.; Wildermuth, M.; Dorer, D.; Cole, J. H.; Rotzinger, H.; Ustinov, A. V. Insulating, Metallic and Superconducting Behavior in a Single Nanowire. *arXiv (Superconductivity)*, June 11, 2020, 2006.06588, ver. 1. https://arxiv.org/abs/2006.06588v1 (accessed 2021 01 05).

ACKNOWLEDGMENTS

The authors thank L. Radtke and S. Diewald of the KIT Nanostructure Service Laboratory for the support concerning the sample fabrication. The work was funded by the Initiative and Networking Fund of the Helmholtz Association, the Helmholtz International Research School for Teratronics (J.N.V. and Y.S.) and the Landesgraduiertenfoerderung (LGF) of the federal state Baden Wuerttemberg (M.W.) and by the German Federal Ministry of Education and Research (BMBF) within the "Research in Photonics" Program (contract number: 13N15016). Further support was provided by the Ministry of Education and Science of the Russian Federation in the framework of the Program to Increase Competitiveness of the NUST MISIS (contract no. K2 2020 022). J.H.C. acknowledges the support of the Australian Research Council Centre of Excellence funding scheme (CE170100039) and the NCI National Facility through the National Computational Merit Allocation Scheme.

REFERENCES

(1) Giordano, N. Evidence for Macroscopic Quantum Tunneling in One Dimensional Superconductors. *Phys. Rev. Lett.* **1988**, *61*, 2137−2140.

(2) Bezryadin, A.; Lau, C. N.; Tinkham, M. Quantum Suppression of Superconductivity in Ultrathin Nanowires. *Nature* **2000**, *404*, 971−974.

(3) Hriscu, A. M.; Nazarov, Y. V. Coulomb Blockade Due to Quantum Phase Slips Illustrated With Devices. *Phys. Rev. B: Condens. Matter Mater. Phys.* **2011**, *83*, 174511.
(4) Astafiev, O. V.; Ioffe, L. B.; Kafanov, S.; Pashkin, Y. A.; Arutyunov, K. Y.; Shahar, D.; Cohen, O.; Tsai, J. S. Coherent Quantum Phase Slip. *Nature* **2012**, *484*, 355−358.
(5) Golubev, D. S.; Zaikin, A. D. Quantum Tunneling of the Order Parameter in Superconducting Nanowires. *Phys. Rev. B: Condens. Matter Mater. Phys.* **2001**, *64*, 014504.
(6) Arutyunov, K.; Golubev, D.; Zaikin, A. Superconductivity in One Dimension. *Phys. Rep.* **2008**, *464*, 1−70.
(7) Langer, J. S.; Ambegaokar, V. Intrinsic Resistive Transition in Narrow Superconducting Channels. *Phys. Rev.* **1967**, *164*, 498−510.
(8) McCumber, D. E.; Halperin, B. I. Time Scale of Intrinsic Resistive Fluctuations in Thin Superconducting Wires. *Phys. Rev. B* **1970**, *1*, 1054−1070.
(9) Kim, H.; Gay, F.; del Maestro, A.; Sacépé, B.; Rogachev, A. Pair Breaking Quantum Phase Transition in Superconducting Nanowires. *Nat. Phys.* **2018**, *14*, 912−917.
(10) Baumans, X. D. A.; Cerbu, D.; Adami, O. A.; Zharinov, V. S.; Verellen, N.; Papari, G.; Scheerder, J. E.; Zhang, G.; Moshchalkov, V. V.; Silhanek, A. V.; van de Vondel, J. Thermal and Quantum Depletion of Superconductivity in Narrow Junctions Created by Controlled Electromigration. *Nat. Commun.* **2016**, *7*, 10560.
(11) Koval, Y.; Jin, X.; Bergmann, C.; Simsek, Y.; Özyüzer, L.; Müller, P.; Wang, H.; Behr, G.; Büchner, B. Tuning Superconductivity by Carrier Injection. *Appl. Phys. Lett.* **2010**, *96*, 082507.
(12) Rotzinger, H.; Skacel, S. T.; Pfirrmann, M.; Voss, J. N.; Münzberg, J.; Probst, S.; Bushev, P.; Weides, M. P.; Ustinov, A. V.; Mooij, J. E. Aluminium Oxide Wires for Superconducting High Kinetic Inductance Circuits. *Supercond. Sci. Technol.* **2017**, *30*, 025002.
(13) Maleeva, N.; Grünhaupt, L.; Klein, T.; Levy Bertrand, F.; Dupre, O.; Calvo, M.; Valenti, F.; Winkel, P.; Friedrich, F.; Wernsdorfer, W.; Ustinov, A. V.; Rotzinger, H.; Monfardini, A.; Fistul, M. V.; Pop, I. M. Circuit Quantum Electrodynamics of Granular Aluminum Resonators. *Nat. Commun.* **2018**, *9*, 3889.
(14) Grünhaupt, L.; Maleeva, N.; Skacel, S. T.; Calvo, M.; Levy Bertrand, F.; Ustinov, A. V.; Rotzinger, H.; Monfardini, A.; Catelani, G.; Pop, I. M. Loss Mechanisms and Quasiparticle Dynamics in Superconducting Microwave Resonators Made of Thin Film Granular Aluminum. *Phys. Rev. Lett.* **2018**, *121*, 117001.
(15) Schön, Y.; Voss, J. N.; Wildermuth, M.; Schneider, A.; Skacel, S. T.; Weides, M. P.; Cole, J. H.; Rotzinger, H.; Ustinov, A. V. Rabi Oscillations in a Superconducting Nanowire Circuit. *npj Quantum Materials* **2020**, *5*, 18.
(16) Mooij, J. E.; Nazarov, Y. V. Superconducting Nanowires as Quantum Phase Slip Junctions. *Nat. Phys.* **2006**, *2*, 169−172.
(17) Mooij, J. E.; Schön, G.; Shnirman, A.; Fuse, T.; Harmans, C. J. P. M.; Rotzinger, H.; Verbruggen, A. H. Superconductor−Insulator Transition in Nanowires and Nanowire Arrays. *New J. Phys.* **2015**, *17*, 033006.
(18) Likharev, K. K. Superconducting Weak Links. *Rev. Mod. Phys.* **1979**, *51*, 101−159.
(19) Attardo, M. J.; Rosenberg, R. Electromigration Damage in Aluminum Film Conductors. *J. Appl. Phys.* **1970**, *41*, 2381−2386.
(20) Black, J. R. Electromigration— A Brief Survey and Some Recent Results. *IEEE Trans. Electron Devices* **1969**, *16*, 338−347.
(21) Hongisto, T. T.; Zorin, A. B. Single Charge Transistor Based on the Charge Phase Duality of a Superconducting Nanowire Circuit. *Phys. Rev. Lett.* **2012**, *108*, 097001.
(22) Smith, R.; Ambegaokar, V. Weak Localization Correction to the Number Density of Superconducting Electrons. *Phys. Rev. B: Condens. Matter Mater. Phys.* **1992**, *45*, 2463−2473.
(23) Bose, S.; Raychaudhuri, P.; Banerjee, R.; Ayyub, P. Upper Critical Field in Nanostructured Nb: Competing Effects of the Reduction in Density of States and the Mean Free Path. *Phys. Rev. B: Condens. Matter Mater. Phys.* **2006**, *74*, 224502.
(24) Aref, T.; Bezryadin, A. Precise *in Situ* Tuning of the Critical Current of a Superconducting Nanowire Using High Bias Voltage Pulses. *Nanotechnology* **2011**, *22*, 395302.
(25) Kapitulnik, A.; Kivelson, S. A.; Spivak, B. Colloquium: Anomalous Metals: Failed Superconductors. *Rev. Mod. Phys.* **2019**, *91*, 011002.
(26) Allain, A.; Han, Z.; Bouchiat, V. Electrical Control of the Superconducting to Insulating Transition in Graphene Metal Hybrids. *Nat. Mater.* **2012**, *11*, 590−594.
(27) Katsumoto, S. Single Electron Tunneling and Phase Transitions in Granular Films. *J. Low Temp. Phys.* **1995**, *98*, 287−349.
(28) Gantmakher, V. F.; Dolgopolov, V. T. Superconductor−insulator quantum phase transition. *Phys. Usp.* **2010**, *53*, 1.
(29) Beloborodov, I. S.; Lopatin, A. V.; Vinokur, V. M.; Efetov, K. B. Granular Electronic Systems. *Rev. Mod. Phys.* **2007**, *79*, 469−518.
(30) Fazio, R.; van der Zant, H. Quantum Phase Transitions and Vortex Dynamics in Superconducting Networks. *Phys. Rep.* **2001**, *355*, 235−334.
(31) Vogt, N.; Schäfer, R.; Rotzinger, H.; Cui, W.; Fiebig, A.; Shnirman, A.; Ustinov, A. V. One Dimensional Josephson Junction Arrays: Lifting the Coulomb Blockade by Depinning. *Phys. Rev. B: Condens. Matter Mater. Phys.* **2015**, *92*, 045435.
(32) Vogt, N.; Cole, J. H.; Shnirman, A. De Pinning of Disordered Bosonic Chains. *New J. Phys.* **2016**, *18*, 053026.
(33) Cedergren, K.; Kafanov, S.; Smirr, J. L.; Cole, J. H.; Duty, T. Parity Effect and Single Electron Injection for Josephson Junction Chains Deep in the Insulating State. *Phys. Rev. B: Condens. Matter Mater. Phys.* **2015**, *92*, 104513.
(34) Cedergren, K.; Ackroyd, R.; Kafanov, S.; Vogt, N.; Shnirman, A.; Duty, T. Insulating Josephson Junction Chains as Pinned Luttinger Liquids. *Phys. Rev. Lett.* **2017**, *119*, 167701.
(35) Kulik, I. O.; Omel'Yanchuk, A. N. Contribution to the Microscopic Theory of the Josephson Effect in Superconducting Bridges. *JETP Lett.* **1975**, *21*, 96.
(36) Ambegaokar, V.; Baratoff, A. Tunneling Between Superconductors. *Phys. Rev. Lett.* **1963**, *10*, 486−489.
(37) Bose, S.; García García, A. M.; Ugeda, M. M.; Urbina, J. D.; Michaelis, C. H.; Brihuega, I.; Kern, K. Observation of Shell Effects in Superconducting Nanoparticles of Sn. *Nat. Mater.* **2010**, *9*, 550−554.
(38) Bollinger, A. T.; Dinsmore, R. C.; Rogachev, A.; Bezryadin, A. Determination of the Superconductor Insulator Phase Diagram for One Dimensional Wires. *Phys. Rev. Lett.* **2008**, *101*, 227003.
(39) Mooij, J. E.; Harmans, C. J. P. M. Phase Slip Flux Qubits. *New J. Phys.* **2005**, *7*, 219−219.
(40) Grünhaupt, L.; Spiecker, M.; Gusenkova, D.; Maleeva, N.; Skacel, S. T.; Takmakov, I.; Valenti, F.; Winkel, P.; Rotzinger, H.; Wernsdorfer, W.; Ustinov, A. V.; Pop, I. M. Granular Aluminium as a Superconducting Material for High Impedance Quantum Circuits. *Nat. Mater.* **2019**, *18*, 816.
(41) Karlsruher Institute of Technology, Verfahren zum Anpassen des elektrischen Widerstands eines Nanodrahts und Verfahren zum Anpassen des elektrischen Widerstands des Nanodrahts sowie von zumindest einem zusätzlichen Nanodraht oder zusätzlichen Nanodrähten. DE102019106508.9, March 14, 2019.
(42) Deutscher, G.; Entin Wohlman, O.; Shapira, Y. Upper Critical Fields in Granular Superconductors. *Phys. Rev. B: Condens. Matter Mater. Phys.* **1980**, *22*, 4264−4270.
(43) Bachar, N.; Pracht, U.; Farber, E.; Dressel, M.; Deutscher, G.; Scheffler, M. Signatures of Unconventional Superconductivity in Granular Aluminum. *J. Low Temp. Phys.* **2015**, *179*, 83.
(44) Sóñora, D.; Carballeira, C.; Ponte, J. J.; Vidal, F.; Grenet, T.; Mosqueira, J. Paraconductivity of Granular Al Films at High Reduced Temperatures and Magnetic Fields. *Phys. Rev. B: Condens. Matter Mater. Phys.* **2019**, *100*, 104509.